Astronomy & Astrophysics manuscript no. output
May 31, 2024

Supernovae Classification Through NOT (Nordic Optical Telescope) Observations

Abad Martín, Ángela[1]

Astronomy department, Stockholm University, Roslagstullsbacken 21, 114 21 Stockholm
e-mail: angela.abad2000@gmail.com

May 31, 2024

ABSTRACT

Aims. To elaborate the spectral acquisition and classification of the supernovae (SNe) ZTF18aawfqax, ZTF24aambaia and ZTF24aamipnt, previously detected by the Zwicky Transient Facility (ZFT) through photometric techniques. The main purpose consisted of the contribution to the effort of categorization and redshift determination of the sources for the survey's completion.
Methods. The project was carried out through spectroscopic observations conducted remotely from the Nordic Optical Telescope (NOT) in La Palma (Spain), using the ALFOSC instrument to provide a greater wavelength coverage for enhanced spectral features. The classification of the sources was elaborated applying the typing tool `Gelato` for an initial categorization and finally `SNID` for a more reliable spectral verification.
Results. According to `Gelato`, it was estimated that ZTF18aawfqax and ZTF24aambai both belonged to the spectral type Ia SNe (62% and 100% probability percentage respectively), whereas ZTF24aamipn was classified as a type II SN. However, according to `SNID`, all the three sources were finally classified as type Ia, coherent with previous categorizations. The redshifts derived from `SNID` (0.054, 0.041 and 0.029, respectively) were also in line with published data.
Conclusions. The consistent spectral categorizations achieved with `SNID` implied this tool provided with higher accuracy results by relying solely on the targets' spectra and comparing them with sources stored in the database. Consequently, these results enhance the catalog of identified SNe from the ZTF, demonstrating the positive outcomes and efficacy of spectroscopic methods followed during the transients observations. In conclusion, this study could contribute to a broader understanding of SNe properties and perhaps serve as a foundation for future research on the possible evolutionary changes within spectra over time, highlighting potential alterations in the physics and chemistry of SNe environments.

Key words. Supernovae (SNe) — Transients — Spectroscopy — Optical — Survey: classification/completeness

1. Introduction

Supernovae (SNe), defined as violent stellar explosions marking the end of their lifespans, have been extensively studied from various angles, not only for their inherent properties but also for their critical involvement in cosmological nucleosynthesis, their impact on the interstellar medium (ISM) and numerous other astronomical phenomena (Filippenko (1997)).

According to Smartt (2009), these events can be classified based on the shape of their spectra, typically observed during their peak brightness phase for these faint point-like sources present brief durations, making them challenging to detect and requiring exceptionally precise observations. On the one hand, type Ia SNe are the result of thermonuclear explosions of white dwarfs and, while lacking hydrogen or helium features, they show Si absorption lines. The physics underlying this particular SNe formation process makes the properties of these sources, such as their peaks luminosities, fairly predictable. That is the main reason why they are usually considered as standard candles and helpful when determining their distances (Gupta (2022)). On the other hand, type II SNe emerge from massive stars ($M_\star \geq 8M_\odot$) that have depleted their fuel and can no longer sustain their core (Hansen (2024a)). These can be sub-divided into type Ib (presenting helium features) or Ic (with no presence of hydrogen nor helium).

Within the scientific community a global effort is underway to secure spectroscopic observations for SNe which had previously been detected using photometric techniques so as to enhance the classification of these events and enable the determination of their intrinsic characteristics. The Zwicky Transient Facility (ZTF) happens to be one of these partnership projects (ZTF (2024)) and our primary goal consists of contributing to the survey's categorization completeness by elaborating a spectral classification for some of their identified transients. This way, employing spectroscopic techniques with the use of the 2.56m diameter Nordic Optical Telescope (NOT) and the implementation of the ALhambra Faint Object Spectrograph and Camera (ALFOSC) instrument at the Observatorio del Roque de los Muchachos (ORM) in La Palma (Spain) (NOT (2024)), we observed several SNe events in distant-mode (see Section 2).

Throughout this project, we arbitrarily selected three of our observed sources presenting reasonable raw data: ZTF18aawfqax, ZTF24aambaia and ZTF24aamipnt. After a reduction process was carried out (see Section 3.1), their corresponding classification was facilitated applying typing tools such as `Gelato` and `SNID` (see Section 3.2).

2. Observations

The planning for elaborating the remote observations at the NOT was established between the afternoon of May 6th till the morn-

ing of May 9th. As already stated in Section 1, ALFOSC (ALFOSC (2024b)) was elected as a well-suited instrument for our requirements because it provided a broad wavelength range and thus enabled a wider extent of spectral features, supplying an accurate characterization and classification of our sources. Additionally, ALFOSC was implemented with grism 4 and a slit-width of 1", necessary for the acquisition of optimized data with medium resolution. This approach was required by our engagement with faint targets, where the objective was to maximize signal capture while mitigating the influence of cosmic rays to the greatest extent feasible.

The observations were performed in the optical (R-band) and consisted not only of the acquisition of spectroscopic data for the targets (see Table 1) but of the procurement of standard stars' spectra, necessary for the flux calibration during the reduction process (see Section 3.1). The latter were chosen principally according to the values of the targets' airmasses for homogeneity purposes along the analysis, using HD 93521 for the sources measured on May 7th and BD 262606 for the event observed on May 8th (see Table 2). Additionally, we measured three flat fields using halogen lamps for both the targets and standard stars, as well as HeNe arcs.

Param.	**SNe (ZTF...)**		
	18aawfqax	**24aambaia**	**24aamipnt**
Obs. Date	May 7th	May 7th	May 8th
α [h:min:s]	15:39:48.48	19:19:06.01	16:22:29.41
δ [º:':"]	+42:17:43.97	+47:35:51.80	+43:31:20.59
m [mag]	18.7 ± 0.1	18.3 ± 0.1	18.4 ± 0.1
t_{exp} [s]	1800	1800	1800
$t_{obs,UT}$ [h:min]	01:36	03:36	02:02
Airmass	1.03	1.13	1.04

Table 1: SNe parameters retrieved from Hansen & students (2024). The following is shown: observation date, right ascension (α), declination (δ), apparent magnitudes (m, errors estimated from Lasair (2024)), exposure times (t_{exp}), time of observation in UT system ($t_{obs,UT}$) and airmass.

Param.	**Calib. Stars**	
	HD 93521	**BD 262606**
Obs. Date	May 7th	May 8th
α [h:min:s]	10:48:23.5	14:49:02.4
δ [º:':"]	+37:34:13	+25:42:09
m [mag]	7.0	9.7
t_{exp} [s]	2	25
$t_{obs,UT}$ [h:min]	23:07	01:40
Airmass	1.15	1.02

Table 2: Standard stars parameters. The values for right ascension (α), declination (δ), magnitudes (m) and exposure times (t_{exp}) were retrieved from ALFOSC (2024a), whereas the UT time of observation ($t_{obs,UT}$) and the airmasses were obtained from Hansen & students (2024).

Throughout the nights we obtained a reasonable seeing of around 0.7 considering the cloudy weather we were subject to for several occasions along the observation. Consequently, this entailed a continuous rescheduling of the plan in an attempt to get the most valuable and optimal data as possible, always prioritizing the Targets of Opportunity (ToO, events of preference due to their unexpected occurrence and/or scientific significance for a certain project) and the monitoring (regular observations executed for a certain source over a period of time).

3. Analysis and Results

Following the acquisition of the set of spectroscopic data outlined in Section 2, the subsequent step involved the reduction process carried out through the use of the `PyNOT` pipeline (Krogager (2024)).

On the other hand, we developed `Python` programs to calculate some basic parameter results such as the Signal to Noise Ratio (SNR) of the spectra, as well as the absolute magnitudes, redshifts and distances of the sources. Finally, the spectral classification was firstly obtained through the use of `Gelato` (Harutyunyan et al. (2008)) as an initial endeavor for identification and was concluded with the verification from `SNID` (Blondin & Tonry (2011)).

3.1. Reduction Procedure

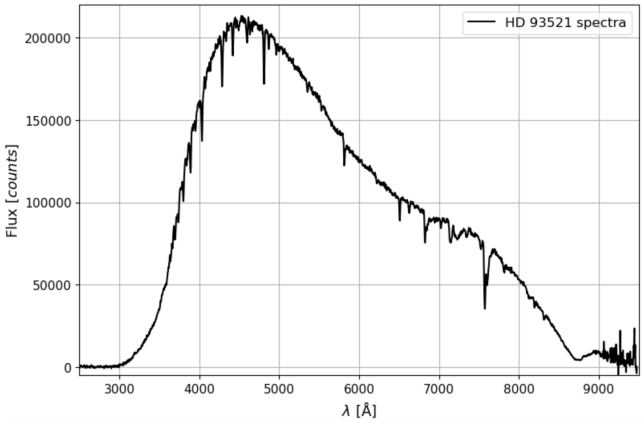

(a) HD 93521

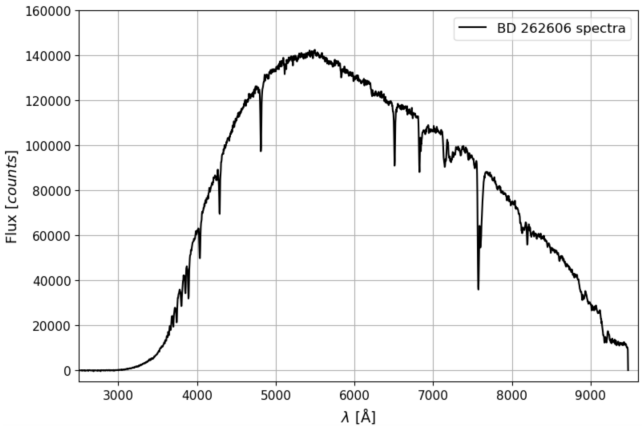

(b) BD 262606

Fig. 1: Reduced spectra for the standard stars (data retrieved from the `PyNOT` pipeline and represented using `Python`), showing the flux (counts) as a function of wavelength (Å).

The reduction process started with the input of each source's data into the `PyNOT` pipeline. The program automatically searches for each data-file, classifying them according to their type and, while it mechanically elaborates master frames to apply for the first reduction steps, it requires a further manual analysis.

This one began with the standard stars' calibration where we had to select the signal out of a System Point Spread Function (SPSF) plot and carefully fit and subtract for any potential background contribution. The axis ranges for the plot could also be modified according to the signal requirements and finally spectral traces and median filter points were fitted in order to diminish the dispersion of the individual values that made up the selected spectrum. As a result, we obtained the finally reduced spectra for the standard stars (see Fig. 1), used automatically by the pipeline along the steps regarding the flux calibration for our target sources.

Next step consisted of the conversion from pixels to wavelength values through the use of HeNe arcs. The procedure was based on the identification of spectral lines with their corresponding x-position, which for `PyNOT` had units of pixels but for arc maps (Hansen (2024b)) had units of Å. By comparing these two, a proper labeling could be achieved.

Lastly, we had to extract the spectra for the SNe targets we were initially interested in classifying. Since the flux calibration and wavelength identification had already been performed, the ultimate stage consisted of repeating the same background subtraction and fitting procedure as the one employed for the standard stars, which led us to the acquisition of the finally reduced spectra for the SNe (see Fig. 2). As can be easily observed from the results obtained, the spectra showed noticeable noise, which can be attributed to two potential main causes.

On the one hand, it is important to notice that these results were influenced by the standard stars' spectra, which were used throughout the flux calibration process and helped in refining background subtraction. Despite their individual reduction, they still presented noise (for instance, Fig. 1a shows a noisy spectra at longer wavelengths) for manual biases were introduced during their extraction. Therefore, when applying them to their corresponding SNe targets, they could propagate this background noise into their spectra.

Secondly, we must consider the fact that the SNe were faint point-like sources with medium/low resolution and thus reproduced low signal spectra which in fact was even more reduced after the standard stars' contribution (this can be seen by comparing the flux order of magnitude between the targets and the standard stars). Consequently, when going through the targets' reduction process they were more subject to background effects, presenting intense noise features.

3.2. Results

Once the spectra for the different targets were determined, the final phase consisted of the classification of the sources and the calculation of some of their main physical parameters.

For the classification, we initially used the typing tool called `Gelato`, which required for both the spectra and an estimation of the redshift of the transient to elaborate its approximate classification. In our case, we inserted the redshift values that had been published in Astronote 2024-124 (2024) as tabulated values (z_{tab}, see Table 3). As a result, we obtained that both ZTF18aawfqax and ZTF24aambaia were classified as type Ia SNe with a 62% and 100% probability, respectively. On the other hand, ZTF24aamipnt was classified as type II (see Table 3).

Since this classification differed for the last source in comparison to the categorization that had been published in Astronote 2024-124 (2024) and Astronote 2024-125 (2024), we decided to elaborate a second identification procedure applying the `SNID` tool. Unlike what happened before, `SNID` simply demanded for the spectra of the sources and it automatically compared it with a sample of already stored and classified SNe that it had so as to obtain the best match. During that process, it did not only categorize the SNe into their spectral type, but suggested their corresponding redshifts, which are the ones we use for the parameter calculations that follow next (z_{exp}, see Table 3).

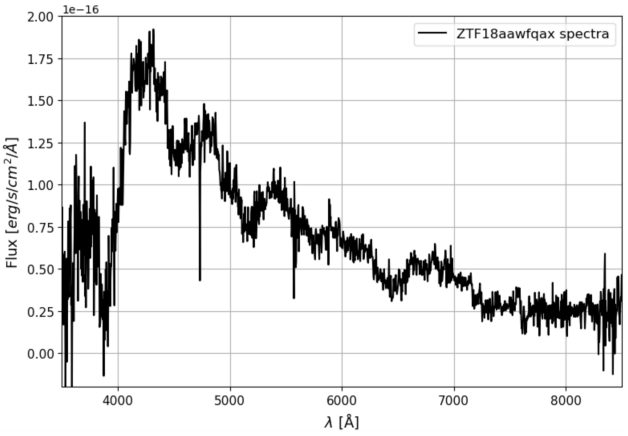

(a) ZTF18aawfqax

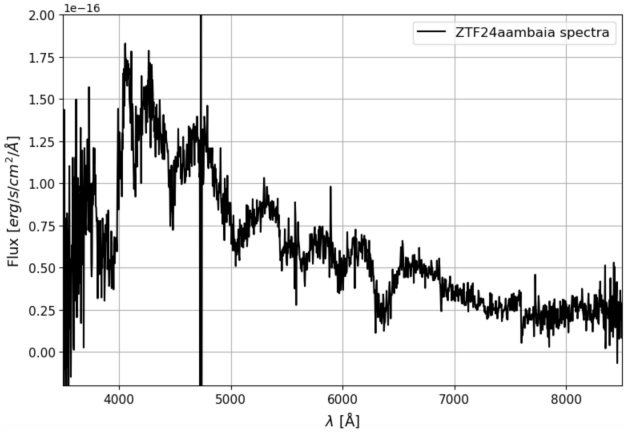

(b) ZTF24aambaia

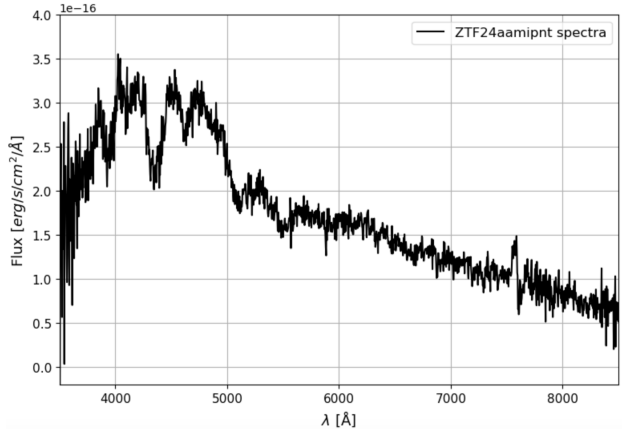

(c) ZTF24aamipnt

Fig. 2: Reduced spectra for the SNe (data has been retrieved from the `PyNOT` pipeline and represented using `Python`), showing the flux (erg/s/cm^2/Å) as a function of wavelength (Å).

It is important to state that these z_{exp} were also estimated from a comparison with the redshifts belonging to their stored data. This way, we finally obtained that all the three targets belonged to the spectral type Ia (see Fig. 3 and Table 3).

From this, we concluded that SNID proved to be a more accurate and realistic SNe classifier. It operated solely based on the input spectrum, making classifications and redshift determinations through comparison and matching procedures with stored spectra from previously categorized sources, thus lowering additional biases. In contrast, GELATO's capability was significantly less robust due to its reliance on additional data (i.e. redshifts) that astronomers may not present initially.

On the other hand, from the experimental redshifts obtained we estimated the approximate distances at which the targets were. According to the Hubble-Lemaître law (Cimatti et al. (2019)), the relative speed at which an astronomical source (i.e. the SNe) at a certain distance (d) moves with respect to an observer at the present time (t_0) is given by:

$$v = H_0 d \tag{1}$$

where H_0 represents the Hubble constant ((67.4 ± 0.5) km/s/Mpc, Aghanim et al. (2020)). Assuming the case of a flat and homogeneous universe for low-redshift sources (as in our case, see Table 3) we can rewrite Eq.(1) as the Hubble's law (Ryden (2017))

$$d \approx \frac{cz}{H_0} \tag{2}$$

with c the speed of light ($3{\cdot}10^8$ m/s).

Additionally, the absolute magnitudes can be computed out of the experimental values obtained for the distance to the transients (see Eq. (2)) and the tabulated values for their apparent magnitudes (m, see Table 1) as follows (Cimatti et al. (2019))

$$M = m - 5log_{10}\left(\frac{d}{pc}\right) + 5 \tag{3}$$

where a negligible dust extinction has been assumed for simplicity purposes.

Finally, the corresponding SNR associated to each of the SNe spectra were also estimated. According to Chromey (2016), the SNR for a Poissonian distribution like ours (where we were essentially counting arriving photons in a CCD), is given by

$$SNR = \frac{\mu}{\sigma_{poiss}} \tag{4}$$

where μ represents the mean of the signal and σ_{poiss} is the standard deviation. Since for this type of distribution it is also true that $\sigma^2_{poiss} = \mu$ with $\mu = N_e$ (where N_e is the number of electrons excited due to the impact of the photons in the CCD, assuming that each photon excites a single electron for simplicity purposes), then we arrive at

$$SNR = \frac{\mu}{\sqrt{\mu}} = \sqrt{\mu} = \sqrt{N_e} \tag{5}$$

However, the finally reduced spectra (which also had low signal due to the effects of the standard stars) had fluxes in units of erg/s/cm^2/Å. Therefore, in order to approach this problem, we firstly decided to acquire their spectra once again avoiding the calibration star process so as to obtain fluxes in units of counts.

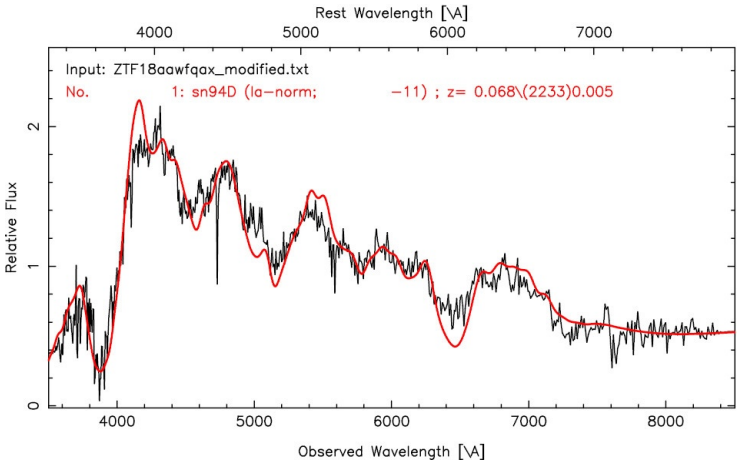

(a) ZTF18aawfqax

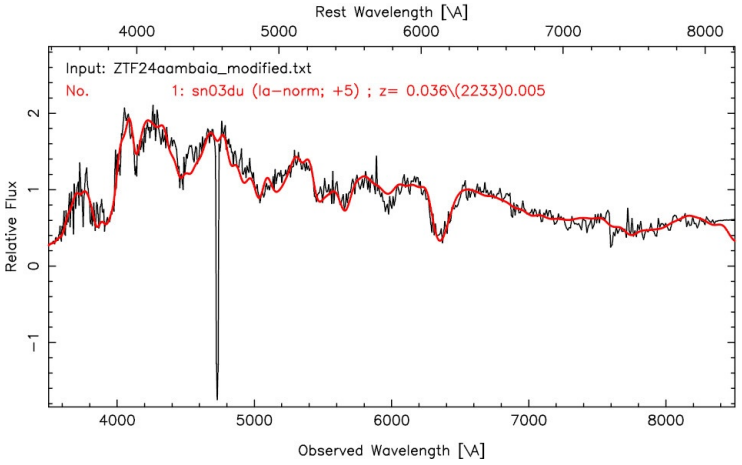

(b) ZTF24aambaia

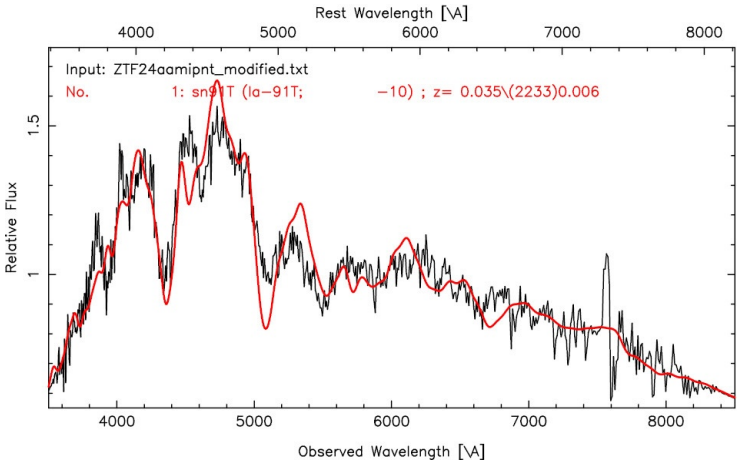

(c) ZTF24aamipnt

Fig. 3: Matching and classification of the SNe spectra using SNID. The figures represent the relative fluxes (dimless.) with respect to the rest and observed wavelengths (Å). Beware that the red values correspond to the best match from the stored data that the program finds for each of our targets, thus the red parameters do not belongs to the analyzed transients in this project.

Afterwards, we decided on the characterization of the SNR in two different spectral ranges (around 4740Å and 7770Å, both covering a scope of roughly 50Å) for it would provide a more constrained and complete analysis. Once the mean counts were calculated withing each wavelength range for each spectra we obtained N_{counts} (in ADU unis). Therefore, in order to finally acquire N_e, we had to multiply the number of counts by the gain of the telescope (0.16 e^-/ADU) and applying Eq. 5 we procured the final estimations for the SNR in each spectrum (see Table 3).

It is crucial to note that all the uncertainties calculated along this section were derived through propagation methods as follows

$$\delta d \approx \left| -\frac{cz}{H_0^2} \right| \cdot \delta H_0 \tag{6}$$

$$\delta M = \delta m + \left| -\frac{5}{ln(10) \cdot d} \right| \delta d \tag{7}$$

Results	SNe (ZTF...)		
	18aawfqax	**24aambaia**	**24aamipnt**
SN Type (Gelato)	Ia (62%)	Ia (100%)	II (unreliable)
SN Type (SNID)	Ia	Ia	Ia
z_{tab}	0.054	0.045	0.03
z_{exp}	0.054	0.041	0.029
d [Mpc]	240.2 ± 1.8	182.4 ± 1.4	129 ± 1
SNR (≈ 4740Å)	20.5	18.5	27.7
SNR (≈ 7770Å)	12.6	10.9	18.0
M [mag]	-18.2 ± 0.1	-18.0 ± 0.1	-17.2 ± 0.1

Table 3: Compilation of final SNe results. The following is shown: SN classification according to `Gelato` and `SNID`, estimated results for the redshifts through the `SNID` classification (z_{exp}), tabulated values for the redshift (z_{tab}) for comparison reasons, estimated distance of the sources (d), Signal to Noise Ratio of the spectra (SNR) and the experimental absolute magnitudes (M).

4. Discussion

In this study, we aimed to observe and detect different SNe events with the main purpose to aid throughout their classification procedure. Given the unfortunate and variable climatic conditions experienced during the observing nights, coupled with the relatively faint nature of our point-like sources compared to the calibration stars used for the flux normalization, our principal findings consisted of some reduced and faint SNe spectra (see Fig. 2) with noticeable noise levels despite having had the background contribution suppressed and being corrected for the telescope's and CCD's inhomogeneities with flat and bias frames.

Subsequently, an individual classification was performed for each spectrum using two different instruments. Initially, a more unrefined tool (`Gelato`) was employed, which required an approximate initial redshift input for the appropriate categorization of each source. With this technique we obtained that while ZTF18aawfqax and ZFT24aambaia were classified as type Ia SNe with a 62% and 100% chance respectively (consistent with the classification done by Astronote 2024-124 (2024)), ZTF24aamipnt was identified as a type II SNe (which differed from the results obtained by Astronote 2024-125 (2024)). Due to this inconsistency, as well as the observation that the latter spectrum did not bore any resemblance to typical type II SNe spectra, usually characterized with distinctive hydrogen spectral lines (this can be verified, for instance, by comparing our result to the type II SNe discovered by AstroNote 2024-5 (2024)), we opted to switch to an alternative tool (`SNID`). This one required only the target spectrum and automatically provided not only a categorization but also an estimated redshift for our source (which we assumed as our experimental value, see z_{exp} in Table 3) based on an extensive comparison with various pre-analyzed SNe stored and classified in its database. This yielded a significantly more precise outcome, grounded in reduced biases, and providing an ultimate identification with all our targets belonging to type Ia SNe.

With respect to the redshift acquisition, clear consistency was observed between the experimental results obtained through our `SNID` classification (which, in turn, relied on our data reduction procedure) and those characterized by Astronote 2024-124 (2024) and Astronote 2024-125 (2024) (see Table 3). Additionally, it is noteworthy that although type Ia systems may appear to be more prevalent during astrophysical observations, this does not necessarily imply their predominance throughout the universe. Furthermore, it is worth highlighting the possibility for a reclassification of these same targets over time, with potential variations in their spectral features based on their intrinsic physical and chemical evolutionary paths during their lifespans.

Based on redshift results, an approximate estimation was obtained for the distances of the targets by applying equations Eq. (2) and (6). Additionally, an approximation for the absolute magnitudes was derived using Eq. (3) and (7) , assuming a negligible value for the extinction factor for simplicity purposes. Consequently we organized the sources from the brightest and farthest to the faintest and closest reading from left to right in Table 3.

Finally, the SNR for the targets was derived in an attempt to detect the noise relevance withing our signals and provide a criterion for verifying the quality of the spectra. As indicated in Section 3.2, estimations were performed in two wavelength ranges for completion and consistency purposes, obtaining values ranging from around 10 to 30 depending on the source and the spectral region evaluated (see Table 3). This results suggested that despite their first-glance appearance, our spectra had an appropriate level of noise, agreeing with previous studies such as that of Smith et al. (2018), where they estimated a SNR(6500Å)≈ 130 pix^{-1} doing spectroscopy with ALFOSC, which translates to a SNR ≈ 21 by multiplying with the gain. It is also significant to mention that for ZTF24aamipnt the SNR may appear higher (see Table 3) due to improper practices, probably presenting a lower magnitude and thus brighter spectrum than expected. The climatic conditions at the time of observation may also be key to explaining why its SNR is significantly greater for this source than for the rest.

To conclude, it is crucial to state that our reduction analysis purely relied on visual and manual uncertainties based on how precisely adjustments were made in `PyNOT`. Additionally, the observation planning was not only subject to clouds, but the time allocated to the priority detection of monitoring and ToO, leaving less room for error for our desired sources when it came to the possibility of repeating measurements or changing targets for better visibility conditions. Furthermore, we remark on our contribution to the classification and completion of the ZTF project, hoping to have facilitated the comprehension of these events and we propose for future observations of the targets to verify the potential evolution of their spectra. Higher resolution approaches

are not suggested since the sources' signals tend to be so faint we doubt any further features could be enhanced.

5. Summary

This project focuses on the detection and classification of SNe spectra belonging to three events detected by the ZTF experiment (ZTF18aawfqax, ZTF24aambaia and ZTF24aamipnt), to further enhance the survey's completeness. Through remote spectroscopic observations conducted at the NOT, equipped with the ALFOSC instrument (see Section 2 for details on the observation planning), and carrying out a meticulous reduction process applying the `PyNOT` pipeline (computational procedure detailed in Section 3.1), the corresponding processed and corrected spectra were obtained (see Section 3.2).

Subsequently, the SNe classification was performed, commencing with the use of `Gelato` for preliminary results, indicating that both ZTF18aawfqax and ZTF24aambaia were type Ia SNe, while ZTF24aamipnt was identified as type II. Additoinally, a more reliable verification was elaborated with `SNID`, classifying all three SNe as type Ia, consistent with previous categorizations. This alignment is particularly valuable as these SNe serve as standard candles, useful for deriving their distances from their redshifts (also in line with published data), reinforcing the reliability of our results. Finally, absolute magnitudes and SNRs were also computed, leading to the discussion about the accuracy of the spectra signals and the appropriate values obtained compared to other studies.

The study encountered challenges, particularly during the observations due to unfavorable climate conditions and during the reduction process, accounting for uncertainties based on visual errors, affecting the noise and background calibration. However, we ended up acquiring remarkably precise estimates aligning with literature results. Overall, we highlight the classification contribution to the ZTF project and suggests for future observations on the targets in an effort to confirm the potential evolution of their spectra and investigate for any changes in the SNe characteristics over their lifespans.

Acknowledgements. We sincerely thank the Observatorio del Roque de los Muchachos for enabling the conduct of this observational project during three consecutive nights, contributing to our student experience in the field. Especially to Alba for her patience and time devoted to this project. We also extend our gratitude to Terese Thidemann as well as the research group and doctoral students working at the ZTF for the opportunity to contribute to the assignment as well as for their guidance and support.

References

Aghanim, N., Akrami, Y., Ashdown, M., et al. 2020, Astronomy & Astrophysics, 641, A6
ALFOSC. 2024a, ALFOSC spectroscopic flux-standard stars, Nordic Optical Telescope, Observatorio el Roque de los Muchachos, La Palma, Spain, https://www.not.iac.es/instruments/alfosc/fluxstandard.html
ALFOSC. 2024b, The ALFOSC page, Nordic Optical Telescope, Observatorio el Roque de los Muchachos, La Palma, Spain, https://www.not.iac.es/instruments/alfosc/
Astronote 2024-124. 2024, Spectroscopic classification of transients, Transient Name Server, https://www.wis-tns.org/astronotes/astronote/2024-124
Astronote 2024-125. 2024, Spectroscopic classification of transients, Transient Name Server, https://www.wis-tns.org/astronotes/astronote/2024-125
AstroNote 2024-5. 2024, FYSE Spectroscopic Classification of Transients with GMOS, Transient Name Server, https://www.wis-tns.org/astronotes/astronote/2024-5
Blondin, S. & Tonry, J. L. 2011, Astrophysics Source Code Library, ascl–1107
Chromey, F. R. 2016, To measure the sky: an introduction to observational astronomy (Cambridge University Press)
Cimatti, A., Fraternali, F., & Nipoti, C. 2019, Introduction to galaxy formation and evolution: from primordial gas to present-day galaxies (Cambridge University Press)
Filippenko, A. V. 1997, Annual Review of Astronomy and Astrophysics, 35, 309
Gupta, R. P. 2022, Monthly Notices of the Royal Astronomical Society, 511, 4238
Hansen, T. T. 2024a, Course session 3, Lecture 3, Observational Astrophysics II, Stockholm University, Sweden, retrieved from Athena, https://athena.itslearning.com/
Hansen, T. T. 2024b, Course session 4. Arc Maps, Observational Astrophysics II, Stockholm University, Sweden, retrieved from Athena, https://athena.itslearning.com/
Hansen, T. T. & students. 2024, Obs_schedule_log2024.xlsx, Observational Astrophysics II, Stockholm University, Sweden, retrieved from Athena, https://athena.itslearning.com/
Harutyunyan, A., Pfahler, P., Pastorello, A., et al. 2008, Astronomy & Astrophysics, 488, 383, https://gelato.tng.iac.es
Krogager, J.-K. 2024, PyNOT-redux, GitHub repository, https://github.com/jkrogager/PyNOT
Lasair. 2024, Latest ZTF Transient Alerts, https://lasair-ztf.lsst.ac.uk
NOT. 2024, Nordic Optical Telescope, Observatorio el Roque de los Muchachos, La Palma, Spain. https://www.not.iac.es
Ryden, B. 2017, Introduction to cosmology (Cambridge University Press)
Smartt, S. J. 2009, Annual Review of Astronomy and Astrophysics, 47, 63
Smith, A., Cabrera, J., Csizmadia, S., et al. 2018, Monthly Notices of the Royal Astronomical Society, 474, 5523
ZTF. 2024, Zwicky Transient Facility, https://www.ztf.caltech.edu